HELICITY COMPUTATION USING OBSERVATIONS FROM TWO DIFFERENT POLARIMETRIC INSTRUMENTS

S.D. BAO[1], A.A. PEVTSOV[2], T.J. WANG[1], and H.Q. ZHANG[1]
[1] *Beijing Astronomical Observatory/National Astronomical Observatories, Chinese Academy of Sciences, Beijing 100012, China*
[2] *Department of Physics, Montana State University, Bozeman, MT 59717, U.S.A.*

(Received 26 November, 1999; in revised form 21 March, 2000)

Abstract. We compare vector magnetograms of active region NOAA 5747 observed by two very different polarimetric instruments: the imaging vector magnetograph of Huairou Solar Observing Station (HSOS) and the Haleakala Stokes Polarimeter of Mees Solar Observatory (MSO). Unlike previous comparative studies, we concentrate our attention on differences in observations and data reduction techniques that can affect the helicity computation. Overall, we find a qualitative agreement between the HSOS and MSO vector magnetograms. The HSOS data show slightly higher field strength, but the distribution of inclination angles is similar in measurements from the two instruments. There is a systematic difference (up to $\sim 20°$) in the azimuths of transverse fields, which is roughly proportional to the longitudinal field strength. We estimate that Faraday rotation in the HSOS magnetograms contributes $\sim 12°$ in the azimuth difference if possible sources of error are taken into account.

Next, we apply two independent methods to both data sets to resolve 180° azimuth ambiguity and to compute two helicity measures — the force-free field parameter α_{best} and the current helicity fractional imbalance ρ_{h}. The methods agree reasonably well in sign and value of the helicity measures, but the HSOS magnetograms show systematically smaller values of ρ_{h} and α_{best} in agreement with an expected contribution of Faraday rotation.

Finally, we discuss the role of Faraday rotation in computation of α_{best} and ρ_{h} and conclude that it does not affect the strength of the hemispheric helicity rule. The strength of the rule appears to be related to a helicity parameter: α_{best} shows weaker hemispheric asymmetry than ρ_{h}.

1. Introduction

Recent work on the helicity of magnetic fields observed at the solar surface demonstrated a preferred sign of helicity, or chirality, in each hemisphere. Based on the Mees Solar Observatory (MSO) data Pevtsov, Canfield, and Metcalf (1995) studied the linear force-free field factor α for 69 active regions, and found that 76% of regions in the northern hemisphere had negative α and 69% in the southern hemisphere had positive α. An extended HSP dataset, using 203 active regions, showed that 62% of regions in the northern hemisphere had negative α and 66% in the southern hemisphere had positive α (Longcope, Fisher, and Pevtsov 1998). Using the Huairou Solar Observing Station (HSOS) vector magnetograms, Bao and Zhang (1998) computed the fractional imbalance of current helicity ($\rho_{\rm h}$) for 422 active regions. In their dataset, 84% of the active regions in the northern hemisphere had negative current helicity, and 79% in the southern hemisphere had positive $\rho_{\rm h}$.

The strength of the hemispheric helicity rule is important for understanding the origin of helicity on the Sun. Still, two data sets reveal a slightly different tendency. The hemispheric asymmetry in the sign of helicity seems to be stronger in the HSOS data. What causes it? Can the differences in the observations and the data reduction explain it, or it is mostly due to the different helicity parameters used in the two studies?

The HSOS magnetograph is a filter-based polarimeter. It observes simultaneously a large spatial area in a single wavelength band (0.125 Å), selectable within a limited range by tuning the filter. Similar (in principle) filter vector magnetographs operate at Marshall Space Flight Center (MSFC) and Big Bear Solar Observatory (BBSO). The MSO Haleakala Stokes Polarimeter is a spectrograph-type magnetograph, which observes an extended spectral range with high spectral resolution at a single spatial point at a given moment. It scans the solar image to build a magnetogram. Several studies compared these two types of magnetographs and showed qualitative agreement between magnetograms derived from them (e.g., Ronan *et al.* 1992; Wang *et al.* 1992). Recently, Hagyard and Pevtsov (1999) compared the linear force-free field α coefficient for several active regions observed by the MSFC and MSO magnetographs and found no significant difference. They also pointed out potential problems in filter vector magnetograph data that could affect the calculation of helicity. Leka and Skumanich (1999) tested three different methods to calculate the parameter α and discussed the influence of data noise on the results. The value of α was computed (1) using moments of the distribution of $\alpha(x, y)$, (2) as the slope of linear function $J_{\rm z}(x, y) = \alpha B_{\rm z}(x, y)$ and (3) as the constant-α force-free field most closely matching the observed horizontal field. All three methods were found to be consistent within the uncertainties.

Thus, in principle, both the observational technique and the data analysis method may contribute to the above-mentioned disagreement between the HSOS and MSO data sets on a strength of the hemispheric helicity rule. In the present paper, we study the relative importance of these factors via direct comparison of magnetograms and the helicity parameters computed from them using different methods. Section 2 describes the instruments and the data sets. Sections 3 and 4 compare magnetic field, electric current and helicity computed using the HSOS and MSO data. Section 5 summarizes the results of our study and the discussion.

2. Polarimetric Observations

2.1. Huairou Vector Magnetograph

The Solar Magnetic Field Telescope at HSOS of Beijing Astronomical Observatory was developed by Ai and Hu (1986) and has made valuable vector magnetic field measurements for more than one decade. The current system consists of a 35 cm vacuum telescope, a 1/8 Å Lyot birefringent filter with three sets of KD*P crystal modulators, a CCD camera with 512×512 pixels, and an image processing system controlled by a computer. It uses the Fe I 5324.191 Å line with a total half-width of 0.334 Å (Landé factor $g_L = 1.5$). The spectral line is formed approximately at 180 km in the solar photosphere (e.g., Lin, Zhang, and Zhang 1996). Because the line is strong and broad, magnetic saturation and Doppler shifts are disregarded. The effective field of view is $5.23' \times 3.63'$. The temporal and spatial resolution of the HSOS vector magnetograms depends on the number of video frames that are added to produce them. Each magnetogram used in this paper is the sum of 256 individual frames for both line-of-sight and transverse fields, corresponding to a temporal resolution of about 5 min and a spatial resolution of about 2 arc sec.

A complete vector magnetogram is built up using four narrow-band images (filtergrams) of Stokes I, V, Q and U parameters. I is derived from the sum of two images, either linearly or circularly polarized. V is a difference between the left and right circularly polarized images taken at -0.075 Å from the line center. Q and U are the differences between two orthogonal linearly polarized images in a certain azimuthal direction. When images for determination of Q and U are taken, the filter is normally switched to the spectral line center to achieve maximum sensitivity. Thus, the observed transverse and longitudinal fields correspond to slightly different heights in the solar photosphere with the longitudinal field originating approximately 50 km lower than the transverse field (Wang *et al.* 1996).

The line-of-sight (B_l) and transverse (B_t) components of magnetic field are given by

$$B_l = C_l \frac{V}{I}, \quad B_t = C_t \left(\frac{Q^2}{I^2} + \frac{U^2}{I^2} \right)^{\frac{1}{4}}, \tag{1}$$

where C_l and C_t are the calibration coefficients. The azimuthal angle of the transverse field is

$$\phi = \frac{1}{2} tan^{-1} \left(\frac{U}{Q} \right). \tag{2}$$

A more detailed description of the instrument and the observational technique may be found elsewhere (e.g., Wang *et al.* 1996).

2.2. Haleakala Stokes Polarimeter

The Haleakala Stokes Polarimeter of Mees Solar Observatory (Mickey 1985) is a spectrograph-based magnetograph which registers full Stokes I, Q, U, and V profiles of the Fe I 6301.5, 6302.5 Å doublet (g_{L}=1.67, 2.5) with high spectral resolution (0.025 Å) and constructs a magnetogram by spatially scanning over the active region targeted. A magnetogram is recorded with a 6″ aperture and either 2.8″ or 5.6″ spatial steps. It takes about an hour to complete a typical magnetogram of 60×40 pixels in spatial extent. The MSO magnetograms used in the present study were obtained with 5.6″ spatial steps. The Fe I 6301.5, 6302.5 Å spectral lines are formed at approximately 200 km in the solar photosphere (e.g., Bruls, Lites, and Murphy 1991).

The magnetic field is computed by combining two inversion techniques. When the fractional polarization in a given pixel is above 1% (corresponding to a field strength $\geq$ 100 G), a nonlinear least-squares fitting technique developed by Skumanich and Lites (1987) is used. The method fits the observed Stokes profiles to the analytical Unno-Rachkovsky solution of the radiative transfer equation. The routine takes into account magnetic filling factor, magneto-optical (e.g., Faraday rotation) and scattered light effects, making a first-order correction for unresolved magnetic structures. In areas of polarization below 1% the field values are determined using integrated properties of the Stokes profiles (Ronan, Mickey, and Orrall 1987). The integral method is based on the same weak-field approximation as Equations (1) and (2), so its accuracy decreases for fields above $\approx$ 1000 G (Canfield *et al.* 1993).

2.3. The Data Sets

We use six vector magnetograms of a single active region NOAA 5747. The region is a complex β-δ spot group with strong magnetic fields and high magnetic shear, which helps to study possible effects of Faraday rotation. The region was well observed by both MSO and HSOS from 19 to 22 October 1989, although there were no simultaneous observations. The smallest time difference between the HSOS and MSO magnetograms is about 8 hours. Table I lists the dates of the observations for both instruments. For each magnetogram, we conduct a transformation to the disk center and resolve the 180° azimuth ambiguity using two independent methods (HSOS and MSO methods, thereafter). In the MSO method the azimuth ambiguity is resolved following Canfield *et al.* (1993), starting from a constant-α force-free field and minimizing change between adjacent pixels, minimazing electric currents in a quiet photosphere. In the HSOS method the ambiguity resolution is done following Wang, Xu, and Zhang (1994) by comparison with a potential field. Both methods are used on both data sets.

3. Magnetic Field and Electric Current

First, we compare three pairs of magnetograms on pixel by pixel basis (HSOS — MSO): 20-Oct/01:37 UT — 20-Oct/17:41 UT, 21-Oct/02:15 — 20-Oct/17:41, and 21-Oct/02:15 — 21-Oct/19:20. For each pair we co-register the HSOS and MSO magnetograms and interpolate the HSOS magnetogram to match the coarser $5.6''$ pixel spacing of the MSO data. The interpolation was done by averaging the HSOS magnetograms over the MSO pixel size. All three pairs show similar correlations. Below we demonstate our findings using the second pair of magnetograms.

3.1. Morphological Comparisons

Figures 1–3 show vector magnetic field, vertical electric current density $J_z = (\nabla \times \mathbf{B})_z$ and current helicity density $(\mu_0 J_z B_z)$, observed by the two instruments. Despite significant time difference (8 hours) between the two observations one can see close similarities in the distribution of magnetic fields and electric currents. In both cases, the orientation of the transverse field (arrows) exhibits a clockwise rotation in the positive (white) polarity field, and counterclockwise rotation in the negative (dark) polarity (upper part of Figure 1). The sense of rotation implies left-hand twist and, hence, negative current helicity density. Indeed, Figure 3 obviously shows that the current helicity density is negative in most of the active region. From this figure, we also see that the distribution of current helicity density is similar between the HSOS and MSO magnetograms.

3.2. Quantitative Analyses

Figure 4 presents a quantitative comparison of two magnetograms shown on Figures 1–3. The scatter plots confirm the results of the morphological comparison. The longitudinal fields correlate quite well, although the HSOS magnetograms exhibit systematically larger longitudinal field strength. In weak field ($|B_l| < 500$ G) the regression coefficient is near 1., and for stronger fields ($|B_l| > 500$ G) it is 0.61. Such a difference is mainly caused by the calibration procedure employed at HSOS (Ai, Li, and Zhang 1982; Wang, Ai, and Deng 1996). For very strong longitudinal fields, the calibration becomes inaccurate. Similarly, the transverse field (Figure 4b) is also systematically larger in the HSOS magnetograms. It is therefore not surprising that the inclination angles of the two magnetograms are in good agreement. The noise level in transverse field measurements, judging from quiet Sun areas, is comparable in the two data sets (200 G for HSOS and 140 G for MSO). In fact, the disagreement in the transverse field strength between HSOS and MSO was also found in other comparisons, as shown in Figure 3b of Ronan *et al.* (1992).

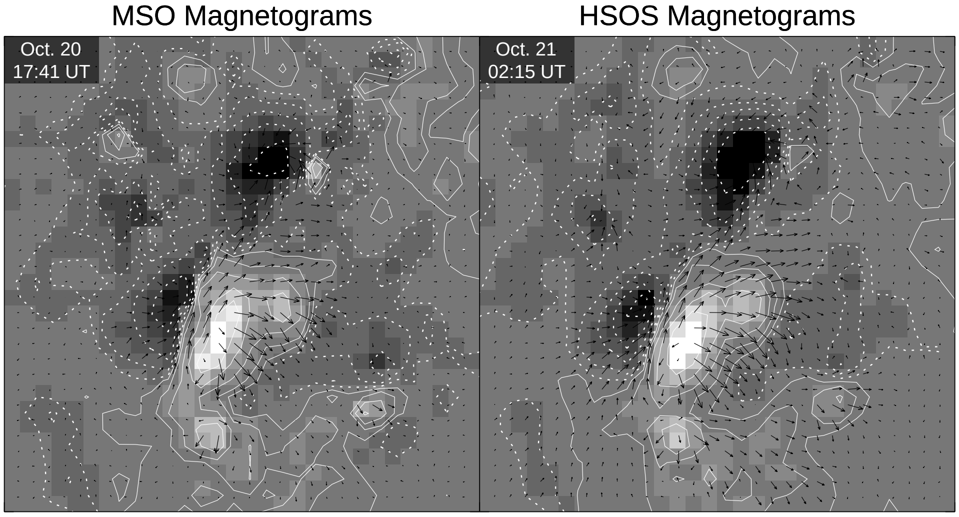

Figure 1. Comparison between a pair of vector magnetograms of AR NOAA 5747 obtained at MSO and HSOS. The MSO magnetogram (left) was recorded with a scan starting at 17:41 UT and ending at 18:37 UT on 20 October 1989. The interpolated HSOS magnetogram (right) was recorded at 02:15 UT on 21 October 1989. The white contours in both maps denote longitudinal field (levels = ± 50, 200, 500, 1000, 1800, and 3000 G); solid and dashed lines show positive and negative fields, respectively. The grey-scale continuum image also shows the intensity of the longitudinal field. The black line segments with arrows indicate the strength and direction of transverse field. The pixel spacing is $5.6''$.

Figure 4d shows the difference in azimuths of the transverse field as a function of the HSOS longitudinal field strength. The linear fit to the data (*dashed line*) reveals a tendency for the difference in azimuths to be negative for the negative longitudinal field and to be positive for the positive field. This tendency may be related to the Faraday rotation effect. In addition, an *average* offset $\sim 20^\circ$ in azimuths can also be seen in the figure.

The random scatter of the magnetic field parameters may be the result of many factors including atmospheric seeing effects, difference in spatial resolution, non-simultaneous observations, and the inability to co-register the two magnetograms perfectly. However, it is difficult to establish how the scatter is apportioned between all the sources of error. The helicity parameters, averaged over all the active region should not be significantly affected in a systematic manner by these random factors. We speculate that Faraday rotation acts in a systematic way, which might alter the helicity computation.

A difference in line formation between the HSOS and MSO data might result in some discrepancies in the azimuths as well. In the MSO data, magnetic field represents a weighted average over the depths of the spectral line formation with the polarized contribution function as weight. In the HSOS

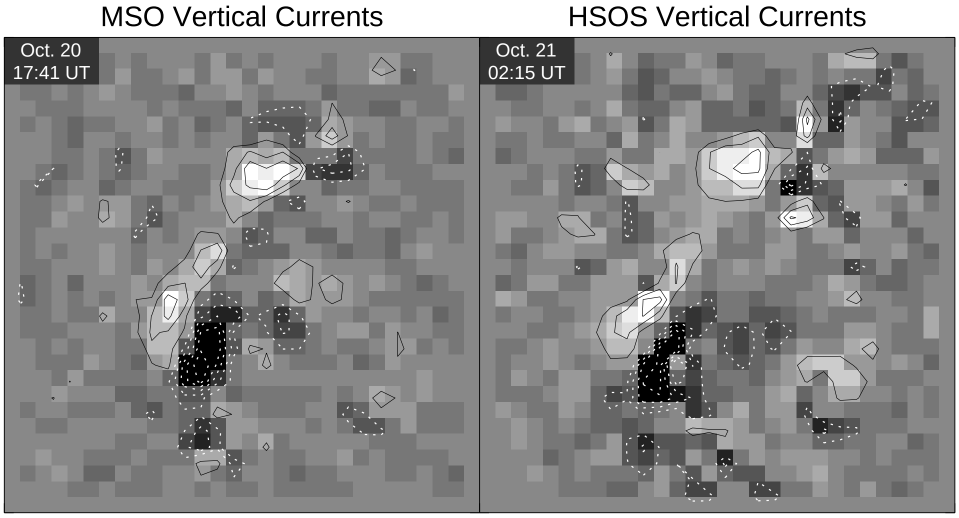

Figure 2. Comparison of vertical current systems derived from two magnetograms of Figure 1. In both maps the vertical currents are contoured at levels of 3, 6, 9, 12, and $15\sigma_{\rm j}$, where $\sigma_{\rm j} = 1.60\,{\rm mA\,m^{-2}}$ for the MSO magnetogram (left) and $\sigma_{\rm j} = 1.81\,{\rm mA\,m^{-2}}$ for the HSOS magnetogram (right). The grey scale also shows vertical currents (white — positive, black — negative).

data, observed magnetic field is the field averaged over the depths covered by the Lyot filter bandpass (0.125 Å). The typical width of the contribution functions is about 150 km for Fe I 5324.191 Å and Fe I 6301.5, 6302.5 Å and it is much larger than the difference in the effective depths of formation of these lines. Hence, we expect that the discrepancies in azimuths due to the difference in depths of formation of the spectral lines will be small. To estimate this discrepancy we use the HSOS magnetogram (21-Oct-89, 02:15 UT) and compute a constant-α force-free field. For each pixel we calculate a difference in azimuths at two levels (0 km — observed magnetogram and $\sim$ 60 km — extrapolated field). For 98% of all pixels the difference is less than 2° and the average is $0.08^\circ \pm 0.77^\circ$.

3.3. Faraday rotation

To further explore the action of Faraday rotation, we overlay the HSOS and MSO magnetograms on Figure 5a. Careful analysis of Figure 5a rules out a *constant* 20° offset between the two magnetograms, since in many areas the HSOS and MSO azimuths are in a good agreement. On the other hand, one can see a tendency of positive difference in azimuths for positive longitudinal field and negative difference for the negative field — further indicates that Faraday rotation is present in the HSOS magnetograms. However, there is another possible source of the difference in azimuths between these two

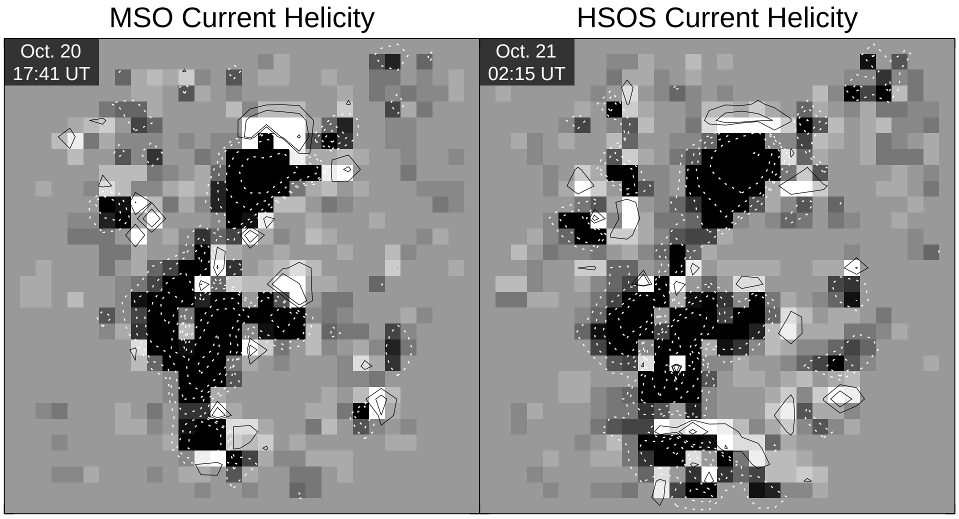

Figure 3. Distribution of the current helicity density $h_c = \mu_0 J_z B_z$ for the magnetograms shown on Figure 1. h_c is shown as the grey-scale image with contours. The contours are drawn at levels of 3, 9, 27, 81, and $243\sigma_h$, where $\sigma_h = 2.32 \times 10^{-3}\,\mathrm{G}^2\,\mathrm{m}^{-1}$ for the MSO magnetogram and $\sigma_h = 2.75 \times 10^{-3}\,\mathrm{G}^2\,\mathrm{m}^{-1}$ for the HSOS magnetogram.

magnetograms. Figure 5b shows an overlay of two HSOS magnetograms observed about 5 hours apart. The white and black line segments represent the transverse fields recorded at 02:15 and 07:00 UT, respectively. Examining the orientation of transverse field in area of strong positive flux (central part of Figure 5b) one can notice a tendency of counterclockwise rotation. The average rotation of the azimuths between the two magnetograms is about 5° over 5 hours. Assuming that the same rotation rate has been present during a period between the MSO and HSOS observations shown on Figure 5a, one can infer that as much as $\sim 8°$ difference in azimuths might be caused by this type of evolution of the sunspot. Remaining $\sim 12°$ should be the result of Faraday rotation. Indeed, comparison of transverse field observed in the center of the spectral line and its blue wings indicates that about 10° in azimuth difference can be caused by the Faraday rotation effect (e.g., Wang *et al.* 1996). This result is in agreement with those estimated by Wang *et al.* (1992).

4. Helicity Parameters

Our next step is to compare helicity parameters computed using two different methods of the ambiguity resolution. For this study we compute three helicity measures: α_{best}, ρ_{h} and $\alpha_{\mathrm{Jz/Bz}}$. The HSOS magnetograms were interpolated to the MSO grid as described in the previous section

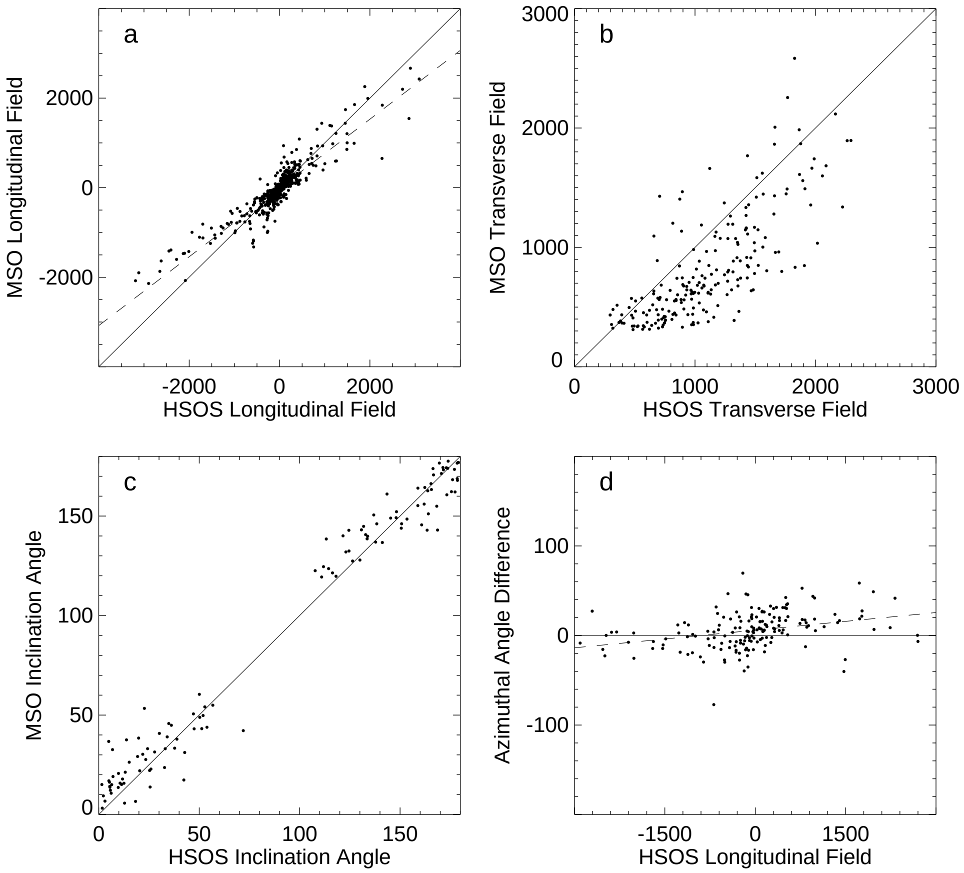

Figure 4. Correlations between magnetic field parameters of the two magnetograms shown on Figure 1. (a) longitudinal field (in G); (b) transverse field (in G); (c) inclination angle (relative to a direction toward observer, degrees); (d) the difference in azimuths as a function of the longitudinal field. Only pixels with transverse field larger than 300 G are included in these correlations. In all the panels, the solid line represents the loci of perfect agreement.

prior to calculating the helicity parameters. $\alpha_{\rm best}$ is computed following Pevtsov, Canfield, and Metcalf (1995), by minimizing the difference between an observed magnetogram and the computed linear force-free field parameterized by $\alpha_{\rm best}$. $\rho_{\rm h}$ is a fractional imbalance of $\mu_0 J_{\rm z} B_{\rm z}$ over an active region (Bao and Zhang 1998). In addition, we define $\alpha_{\rm Jz/Bz}$ as the regression coefficient for the relationship between vertical components of the electric current density ($\mu_0 J_{\rm z}$) and the magnetic induction ($B_{\rm z}$). Pevtsov, Canfield, and McClymont (1997) found a good correlation between $J_{\rm z}$ and $B_{\rm z}$ for this active region, suggesting that the linear force-free field model is a good approximation. All three parameters are computed using only pixels with value of transverse field $B_{\rm t} > 300\,{\rm G}$ and longitudinal field $B_{\rm l} > 20\,{\rm G}$. The

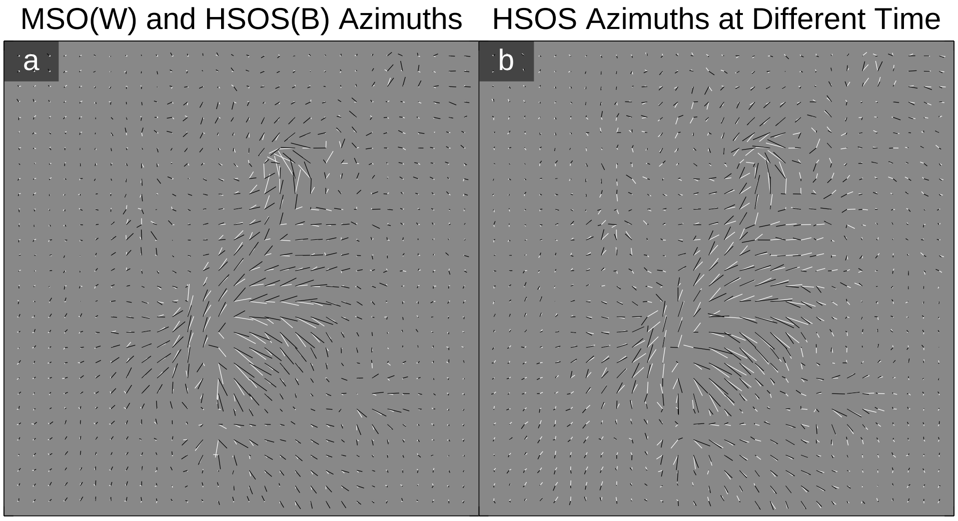

Figure 5. Azimuths of the transverse field of two pairs of magnetograms. (a) MSO and HSOS magnetograms, white segments correspond MSO data (e.g., Figure 1, left), black segments show HSOS magnetogram (e.g., Figure 1, right); (b) two HSOS magnetograms, white segments show the transverse field at 02:15 UT, and the black line segments show the transverse field at 07:00 UT.

results are summarized in Table I. $\alpha_{\rm best}$ and $\rho_{\rm h}$ computed using different methods of the azimuth ambiguity resolution are in good agreement within each set of magnetograms (HSOS or MSO). Thus, for this active region, the results are relatively insensitive to the method of resolution of the 180° azimuth ambiguity. On the other hand, Hagyard and Pevtsov (1999) have shown that for a highly non-potential active region, the azimuth ambiguity resolution method used might affect the value of $\alpha_{\rm best}$.

In the framework of our present comparison, it is important to note that the MSO data give a more robust result since the data are less affected by Faraday rotation. Hence, we compare the HSOS data with the MSO data assuming that the latter give more "correct" answer.

The helicity parameters computed using the HSOS magnetograms are systematically smaller than those using the MSO data. This is an expected contribution of Faraday rotation. Figure 4d (or Figure 5a) demonstrates that Faraday rotation has a stronger effect in the positive polarity field. The effect of Faraday rotation introduces right-hand twist (positive helicity) in positive flux and, hence, decreases the overall negative current helicity density of this active region.

Table I. α_{best} and ρ_{h} in AR 5747.

Date	Time (UT)	$\alpha^1{}_{\mathrm{best}}$	ρ_{h} (%)	$\alpha^1{}_{\mathrm{best}}$	ρ_{h} (%)	$\alpha^1{}_{\mathrm{Jz/Bz}}$
		HSOS method		MSO method		
HSOS data						
19 Oct., 1989	02:42	−4.16	−58.9	−3.52	−57.9	−3.75
20 Oct., 1989	01:37	−3.25	−66.7	−3.99	−74.8	−4.54
21 Oct., 1989	02:15	−4.46	−71.6	−3.65	−69.0	−3.69
MSO data						
20 Oct., 1989	17:41	−6.29	−82.6	−6.33	−82.3	−5.87
21 Oct., 1989	19:20	−5.64	−79.5	−5.15	−79.2	−5.32
22 Oct., 1989	18:27	−4.97	−69.0	−4.84	−72.3	−4.58

[1] in units $10^{-8}\ m^{-1}$

5. Discussion

In the previous section we have shown that the presence of Faraday rotation reduces the value of the helicity parameters for a given active region. An important question is how it affects the sign of helicity.

Figure 6 demonstrates the effect of Faraday rotation in a bipolar active region represented by a twisted flux tube. The vertical box plotted by the dashed lines encompasses an "active region". The two upper panels represent an active region of positive helicity ($\alpha > 0$, right-hand twist). The two lower panels show an active region of negative helicity ($\alpha < 0$, left-hand twist). The middle column represents a twist introduced by Faraday rotation and the last column depicts the combined effect of the original distribution of azimuths and that resulting from Faraday rotation. From this cartoon, one can see that whether its current helicity is positive ($\alpha > 0$) or negative ($\alpha < 0$) for a bipolar active region, the twist in one polarity (panel a or d) strengthens due to Faraday rotation while that in another opposite polarity (panel b or c) weakens. This means that the effect of Faraday rotation will not change the original sign of current helicity in such a region. Now let us assume that the panels a, b, c, and d respectively represent four unipolar active regions with different twists. In the case of a or d, the current helicity sign is not affected by the Faraday rotation effect, even if their values increase to a great extent. For the panel b or c, however, if the magnetic field is current-free (no original twist) or just slightly twisted, the resulting twist will be determined primarily by the action of Faraday rotation.

On the other hand, Hagyard and Pevtsov (1999) argue that Faraday rotation may affect the helicity computation of even bipolar active regions,

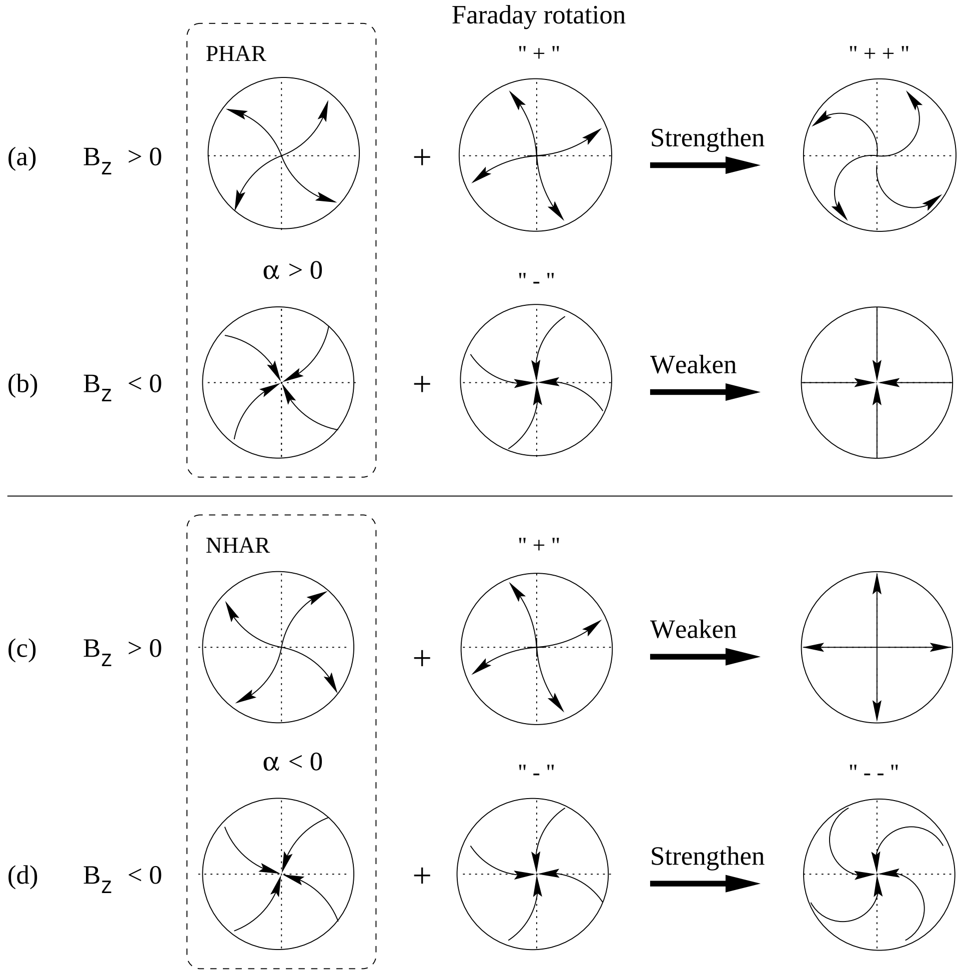

Figure 6. Sketches showing the influence of Faraday rotation action on twisted magnetic flux tubes. The four circles in the first column represent possible configurations of twisted flux tubes. The curves with arrows denote magnetic field lines. The patterns of the second column indicate the sense of the spiral configuration due to Faraday rotation. The sketches of the last column indicate the net effect resulting from the original twist modified by Faraday rotation. The final configuration on panels (b) and (c) depends on the amount of original twist and the Faraday rotation and may be opposite in sign to the original twist.

since the leading polarity sunspot has stronger (and more compact) magnetic field and tends to live longer. Hence, the effect of Faraday rotation will be determined mostly by a leading polarity sunspot. Moreover, because the leading sunspots have opposite polarities in opposite hemispheres (Hale-Nicholson polarity rule) the Faraday rotation may, in fact, influence the hemispheric helicity rule.

Table II. Signs of $\rho_{\rm h}$ and $\alpha_{\rm best}$ for 422 active regions.

Hemisphere	Total of ARs	$\rho_{\rm h}$	$\alpha_{\rm best}$
		Negative chirality	
Northern	199	168 (84%)	152 (76%)
		Positive chirality	
Southern	223	177 (79%)	159 (71%)

However, it is not that simple. Table I shows that Faraday rotation affects both helicity parameters — $\alpha_{\rm best}$ and $\rho_{\rm h}$. Although we studied only one active region, we may speculate that the Faraday rotation has similar effect on both helicity parameters for all active regions. Hence we expect to see the same hemispheric asymmetry in $\rho_{\rm h}$ and $\alpha_{\rm best}$ for the same data set. Table II shows the sign of those two parameters computed for the data studied by Bao and Zhang (1998). Clearly, the hemispheric asymmetry is weaker in $\alpha_{\rm best}$ and stronger in $\rho_{\rm h}$. The strength of the hemispheric helicity rule in MSO and HSOS data sets seems to agree when the same helicity parameter ($\alpha_{\rm best}$) is used.

Thus, despite that Faraday rotation may affect the hemispheric helicity rule, Table II does not support that. It appears that the strength of the hemispheric helicity rule may be determined by a choice of helicity parameters. Authors could not reach a consensus on either there are physical reasons for that (e.g., relation to the different physical processes on the Sun), or that the reasons are methodological in nature (e.g., one parameter is more susceptible to local variations of azimuths than another). Before the contradiction between $\alpha_{\rm best}$ and $\rho_{\rm h}$ is solved we think that both parameters should be used in studies of helicity of the photospheric magnetic field on the Sun.

Acknowledgements

We are grateful to the staff of the two observatories for the observations. We wish to thank R.C. Canfield for valuable discussions. The authors also thank the referee for helpful comments and suggestions. This work was carried out under the support of the National Science Foundation of China grants 19791090 and 49990450, and NASA through SR&T grant NAG5-6110.

References

Ai, G.X. and Hu, Y.F.: 1986, *Acta Astron. Sinica* **27**, 173.
Ai, G.X., Li, W., and Zhang, H.Q.: 1982, *Acta Astron. Sinica* **23**, 39.
Bao, S.D. and Zhang, H.Q.: 1998, *Astrophys. J.* **496**, L43.
Bruls, J.H.M.J., Lites, B.W., and Murphy, G.A.: 1991, in L.J. November, editor, *Solar Polarimetry*, NSO/SP, Sunspot, New Mexico, p. 444.
Canfield, R.C., de La Beaujardière, J.-F., Fan, Y. *et al.*: 1993, *Astrophys. J.* **411**, 362.
Hagyard, M. and Pevtsov, A.A.: 1999, *Solar Phys.* **189**, 25.
Leka, K.D. and Skumanich, A.: 1999, *Solar Phys.* **188**, 3.
Lin Y.Z., Zhang, H.Q., and Zhang, W.J.: 1996, *Solar Phys.* **168**, 135.
Longcope, D.W., Fisher, G.H., and Pevtsov, A.A.: 1998, *Astrophys. J.* **507**, 417.
Mickey, D.L.: 1985, *Solar Phys.* **97**, 223.
Pevtsov, A.A., Canfield, R.C., and McClymont, A.N.: 1997, *Astrophys. J.* **481**, 973.
Pevtsov, A.A., Canfield, R.C., and Metcalf, T.R.: 1995, *Astrophys. J.* **440**, L109.
Ronan, R.S., Mickey, D.L., and Orrall, F.Q.: 1987, *Solar Phys.* **113**, 353.
Ronan, R.S., Orrall, F.Q., Mickey, D.L., West, E.A., Hagyard, M.J., and Balasubramaniam, K.S.: 1992, *Solar Phys.* **138**, 49.
Skumanich, A. and Lites, B.W.: 1987, *Astrophys. J.* **322**, 473.
Wang, H.M., Varsik, J., Zirin, H., Canfield, R.C., Leka, K.D., and Wang, J.X.: 1992, *Solar Phys.* **142**, 11.
Wang, J.X., Shi, Z.X., Wang, H.N., and Lü, Y.P.: 1996, *Astrophys. J.* **456**, 861.
Wang, T.J., Ai, G.X., and Deng, Y.Y.: 1996, *Publications of the Beijing Astronomical Observatory* **28**, 31.
Wang, T.J., Xu, A.A., and Zhang H.Q.: 1994, *Solar Phys.* **155**, 99.